Available online at www.sciencedirect.com

ScienceDirect

International Journal of Solids and Structures 44 (2007) 3720–3737

INTERNATIONAL JOURNAL OF SOLIDS and STRUCTURES

www.elsevier.com/locate/ijsolstr

Determining plastic properties of a material with residual stress by using conical indentation

J. Yan [a], A.M. Karlsson [a,*], X. Chen [b]

[a] *Department of Mechanical Engineering, University of Delaware, Newark, DE 19716-3140, USA*
[b] *Department of Civil Engineering and Engineering Mechanics, Columbia University, New York, NY 10027-6699, USA*

Received 20 July 2006; received in revised form 3 October 2006; accepted 13 October 2006
Available online 20 October 2006

Abstract

Instrumented indentation is a popular method for determining mechanical properties in engineering materials. However, there are several shortcomings and challenges involved with correctly interpreting the test results. We propose here a unified method for evaluating instrumented indentation testing conducted on a material that exhibits both strain hardening under yielding and which is subjected to uniform, equi-biaxial residual stresses. The proposed method is based on extensive finite element simulations that relate the parameter-space spanned by Young's modulus, yield strength, strain hardening and residual stress, to the response from the indentation test. Based on reverse analysis, the proposed method can be used to determine two unknown quantities, such as yield strength and strain hardening. The technique involves utilizing the concept of representative strain and plural indenter-shapes.

Keywords: Indentation; Residual stress; Finite element analysis; Representative strain; Plasticity

1. Introduction

Instrumented indentation has emerged as a popular method to determine the mechanical properties of materials where traditional methods (such as tensile testing) are not convenient to use. For example, coatings and multilayered structures may consist of materials that are not available in bulk, or—when available—the bulk properties may be quite different from the properties of the small sizes associated with layered or coated structures. Moreover, coatings used for thermal protection in high temperature applications, such as gas turbines for propulsion and energy production, evolve as they are exposed to elevated temperatures and can in addition exhibit local compressive mismatch stresses as high as 4-6 GPa at room temperatures, e.g. (Karlsson and Evans, 2001; Karlsson et al., 2002). In this class of applications, the material properties are many times unknown, since the materials only exist as a coating and—in the case of evolving properties—may only exist in a particular form for a relatively short time, e.g. (Chen et al., 2003; Pan et al., 2003). Thus, instrumented

* Corresponding author. Tel.: +1 302 831 6437; fax: +1 302 831 3619.
E-mail address: karlsson@udel.edu (A.M. Karlsson).

0020-7683/$ - see front matter
doi:10.1016/j.ijsolstr.2006.10.017

indentation may be a preferred method to evaluate the properties of such materials, since this technique is relatively simple to perform. Unfortunately, in-spite of its popularity, there are still some challenges involved with evaluating instrumented indentation tests. For example, the most popular method used (Oliver and Pharr, 1992), does not take into account residual stress and the existence of work hardening makes it more difficult to interpret the indentation measurements.

Thus, our aim is to develop a technique that can be used for evaluating indentation tests of a material with significant strain hardening that is also subjected to equi-biaxial residual stress (which is one of the most common forms of residual stress). Before proceeding, we will review the "traditional method" for evaluating indentation tests and discuss related work striving to extend the commonly used method. The discussion will be limited to the more widely used axisymmetric, conical indenters (Johnson, 1985) even though the technique can be easily be extended to spherical indenters and other forms of residual stress. We note that indentation made by a Berkovich or Vickers indenter, results in the same force-displacement curve as a conical indenter with half apex angle, $\alpha = 70.3°$ (Fig. 1) (Cheng and Cheng, 2004; Lichinchi et al., 1998)—the same principle applies to other pairs of sharp pyramid and conical indenters, and also for materials with work hardening and/or residual stress: as long as the depth-cross section area ratio keeps the same, the indentation force-displacement curve measured with a sharp pyramid tip is almost the same as that with a conical indenter. Subsequently, the conical indenter is used in this study to help reducing computational effort.

1.1. A brief review of the indentation technique

In evaluating indentation testing, the indenter is usually assumed as a rigid cone with half apex angle, α, see Fig. 1. In the absence of residual stress and of strain hardening, the classic indentation theory relates the hardness, H, and contact stiffness, S, with the yield strength, σ_y, and Young's modulus, E, for a homogeneous, isotropic bulk material as:

$$H = P/(\pi a^2) = c\sigma_y, \tag{1a}$$

and

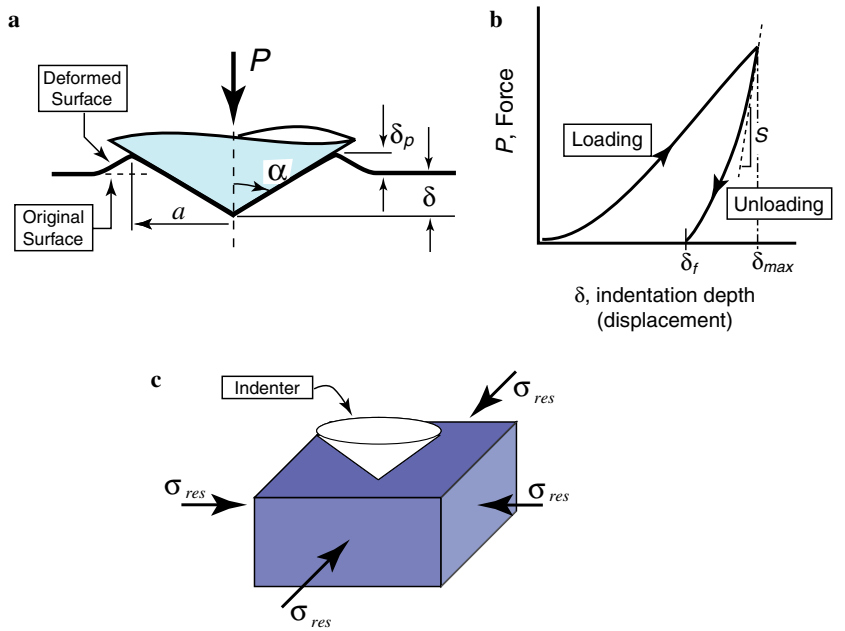

Fig. 1. Schematic illustration of instrumented indentation with a sharp, conical axisymmetric indenter. (a) Indentation of a homogeneous, isotropic, semi-infinite material. (b) A typical load displacement curve obtained from an indentation experiment. (c) Biaxial, residual stress.

$$S = 2\gamma aE/(1-\nu^2). \tag{1b}$$

In Eq (1) σ_y is the yield strength of an elastic-perfectly plastic specimen; for materials with work hardening, it should be replaced by a uniaxial flow stress corresponding to an effective strain of about 0.08–0.1 (Tabor, 1951). S is the slope of the initial portion of the elastic unloading curve (Fig. 1), c is a constraint factor that increases nonlinearly with E/σ_y, $\gamma \approx 1.08$ is a correction factor for the conical indenter, and ν is Poisson's ratio of the homogeneous, isotropic specimen (Hay et al., 1999; Johnson, 1985). Finally, a is the projected contact radius measured at maximum penetration, as indicated in Fig. 1. A common approximation used for determining a is from the expression for the projected contact area, A, for a geometrically perfect conical indenter (Oliver and Pharr, 1992):

$$A = \pi a^2 = 24.5\delta_c^2, \tag{2a}$$

where the contact depth, δ_c, can be determined by (Oliver and Pharr, 1992)

$$\delta_c = \delta_{\max} - \varepsilon\frac{P_{\max}}{S}. \tag{2b}$$

with $\varepsilon = 0.75$ for a Berkovich indenter ($\alpha = 70.3°$ (Oliver and Pharr, 1992))[1] and $\delta_{\max}$ being the maximum indentation depth (Fig. 1). When the indentation depth is sufficiently large, such that the strain gradient effect may be ignored, both hardness and stiffness are independent of the indentation depth[2] (Fleck and Hutchinson, 1997).

There are several disadvantages with the classical theory discussed above, see for example (Cheng and Cheng, 2004). The most critical shortcomings are (i) ignoring the plastic pile-up (or sink-in) at the perimeter of the indentation (Chen et al., 2006); (ii) needing the projected contact area, A (the true contact area can deviate significantly from the estimate); (iii) difficulties to account for the strain hardening effect accurately and (iv) assuming a structure without residual stresses. A significant amount of work aiming to release some of these restrictions can be found in the referred literature, for example (Atkins and Tabor, 1965; Cao and Lu, 2004; Carlsson and Larsson, 2001a,b; Chen et al., 2006; Chollacoop et al., 2003; Dao et al., 2001; Eriksson et al., 2003; Lee and Kwon, 2003, 2004; Ogasawara et al., 2005, 2006a,b; Suresh and Giannakopoulos, 1998; Swadener et al., 2001; Xu et al., 2005; Yan et al., 2007; Zhao et al., 2006a,b).

A common method for considering the effects of residual stresses is to compare the contact depth, contact area and/or force-displacement curves (Carlsson and Larsson, 2001a,b; Lee and Kwon, 2003, 2004; Swadener et al., 2001) of material samples with and without residual stress. Recent work have suggested simplified approaches, where the knowledge of the stress free indentation response is not needed (Chen et al., 2006), with further simplifications that eliminated the need of knowledge about the projected contact area (Yan et al., 2007; Zhao et al., 2006a,b). The effect of strain hardening has also been noted to have a significant effect on indentation testing. An effective method to incorporate strain hardening is to introduce "representative strain." The concept of representative strain was introduced by Atkins and Tabor (Atkins and Tabor, 1965) and has been used by several authors (Cao and Lu, 2004; Chollacoop et al., 2003; Dao et al., 2001) and generalized by Ogasawara et al. (2005, 2006a,b). In the current paper, we will follow the latter approach which is summarized later in this chapter. Interestingly (to the knowledge of the authors), there is no significant work towards combining the effect of strain hardening and residual stress when analyzing of indentation testing, even though several authors have noted that this may be a significant factor, e.g. (Eriksson et al., 2003; Suresh and Giannakopoulos, 1998; Xu et al., 2005).

With the goal of the current paper being to develop a technique that can be used for evaluating indentation tests of a material with significant strain hardening that is also subjected to equi-biaxial residual stress, we will in the following outline some fundamental concepts pertaining to strain hardening and the associated concept of "representative strain," before discussing how this can be combined with residual stress.

[1] Indentation made by a Berkovich or Vickers indenter, results in the same force-displacement curve as a conical indenter with half apex angle, $\alpha = 70.3°$ (Cheng and Cheng, 2004; Lichinchi et al., 1998).

[2] For metals, it is observed that the hardness increases with decreasing indentation depth, when the penetration is in the sub-micron regime. This is known as strain gradient plasticity. Such effects are ignored here, assuming that the indentation depth is sufficiently deep.

1.2. Strain hardening

A typical uniaxial stress-strain curve including both elastic and inelastic responses is shown in Fig. 2. This class of curves is commonly described by a power law:

$$\sigma = \begin{cases} E\varepsilon \text{ for } \varepsilon \leqslant \sigma_y/E \\ R\varepsilon^n \text{ for } \varepsilon \geqslant \sigma_y/E \end{cases}. \tag{3}$$

In Eq. (3), n is the work-hardening exponent and $R \equiv \sigma_y\,(E/\sigma_y)^n$ is the rate of work-hardening. Vanishing n corresponds to linear-elastic, perfectly-plastic material. For most metals and alloys $0.1 \leqslant n \leqslant 0.5$.

Based on dimensional analysis, the following relationship between the indentation force (during loading), displacement, constitutive properties and indenter angle has been suggested for material with strain hardening (Cheng and Cheng, 1998, 2004):

$$\frac{P}{E\delta^2} = \Pi(E/\sigma_y, n, \nu, \alpha), \tag{4}$$

where Π is a dimensionless function. However, Poisson's ratio, ν, may be ignored in indentation analysis (Cheng and Cheng, 1998, 2004; Mesarovic and Fleck, 1999), thus reducing the dependency of the dimensionless function Π to only two material properties and the indenter shape. Π can be determined through extensive finite element simulations, see for example (Cheng and Cheng, 2004). Reverse analysis based on such dimensionless function can then be used to extract the unknown mechanical properties. To reduce the apparent number of unknowns, a "mathematical trick" is commonly used, involving the introduction of the parameters "representative strain" and "representative stress," discussed next.

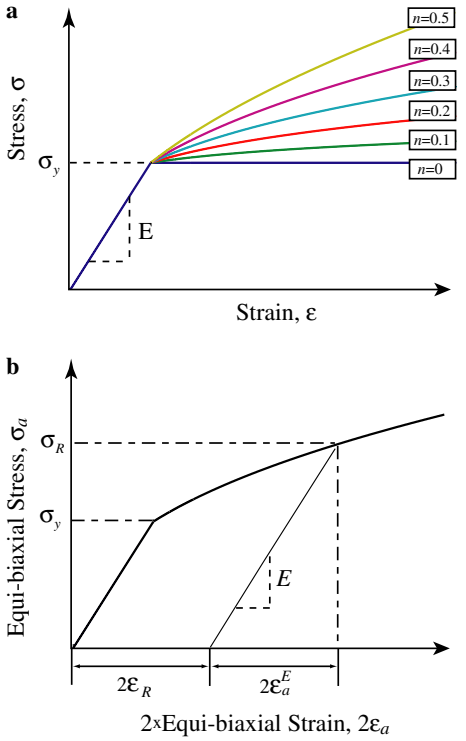

Fig. 2. (a) Typical uniaxial, stress-strain curves following the power-law given in Eq. (3). (b) The equi-biaxial stress strain curve, identifying the representative strain, ε_R, and representative stress, σ_R.

1.3. Representative strain and stress

The concept of representative strain was introduced by (Atkins and Tabor, 1965), was later extended by (Dao et al., 2001), and generalized by (Ogasawara et al., 2005). In general, on the uniaxial stress-strain curve, a representative strain ε_R can be identified and a universal description of the representative stress can be written as

$$\sigma_R\langle\varepsilon_R\rangle = R\left(m\frac{\sigma_R\langle\varepsilon_R\rangle}{E} + 2\varepsilon_R\right)^n. \tag{5}$$

For each m, the value of ε_R is varied such that Eq. (4) effectively loses its apparent dependency of the work-hardening exponent. In other words, with the normalization of the representative stress, the relationship

$$\Phi \equiv \frac{C}{\sigma_R\langle\varepsilon_R\rangle} \equiv \frac{P}{\delta^2\sigma_R\langle\varepsilon_R\rangle} = \Pi_1\left(\frac{E}{\sigma_R\langle\varepsilon_R\rangle}\right) \tag{6}$$

becomes essentially independent of n. Here, $\Phi \equiv C/\sigma_R\ \langle\varepsilon_R\rangle$ corresponds to the normalized indentation load, $C = P/\delta^2$ is the loading curvature, and $\bar{E} = E/(1-\nu^2)$ is the plane strain modulus. Π_1 is the fitting of the numerical results, often expressed by polynomial functions. The R^2 value (R^2) can be computed between the functional fit Π_1 and data points. For a given m, the optimum value of ε_R is identified when R^2 is maximized (closest to 1).

R^2 is plotted as a function of m and $2\varepsilon_R$ in Fig. 3. [Numerical results based on Ogasawara et al. (2005)]. It can be readily seen that the most accurate numerical results (maximum R^2) are obtained when $m = 2$ for a Berkovich indenter, where the best independency of n is obtained for Eq. (6). Therefore, it is shown that—absent residual stress—the optimum value of the representative strain for a Berkovich indenter ($\alpha = 70.30°$) is $\varepsilon_R = 0.0115$ at $m = 2$. The optimum value of m (=2) that leads to the best numerical results (thus takes the most advantage of the representative strain-based indentation analysis) is unchanged when the indenter angle is varied in a moderate range (Ogasawara et al., 2005).

Ogasawara et al. (2005) justified the representative strain obtained from such optimization procedure as the plastic strain of equi-biaxial loading, Fig. 2(b), by assuming small Poisson's effect during elastic deformation. Inspired by the earlier work, here we adopt the same formulation of the representative stress, i.e.

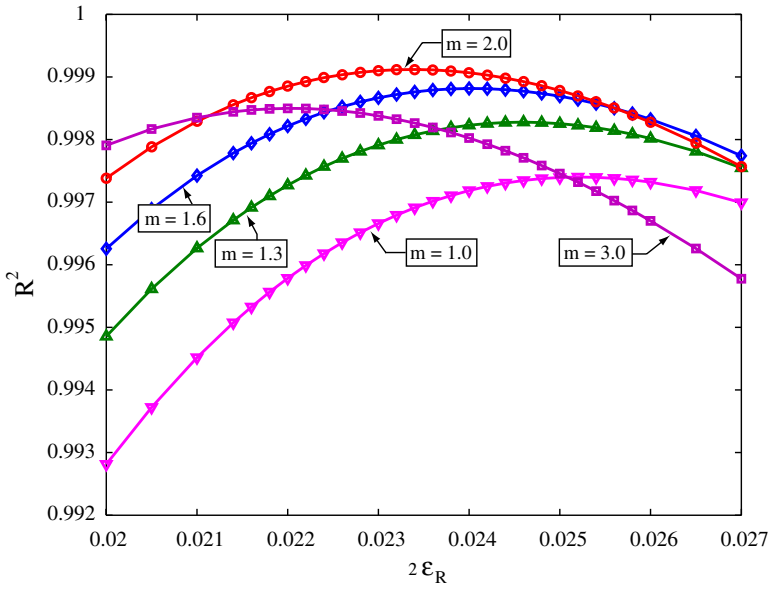

Fig. 3. The R-squared value, R^2, as a function of m and ε_R for $\alpha = 70.3°$. The best numerical results are obtained when $m = 2$ and $2\varepsilon_R = 0.023$ (on the uniaxial stress-strain curve).

$$\sigma_R\langle\varepsilon_R\rangle = R\left(2\frac{\sigma_R\langle\varepsilon_R\rangle}{E} + 2\varepsilon_R\right)^n. \tag{7}$$

When residual stress is taken into account, for a given indenter shape (i.e. α is known) and at a give residual stress level σ_{res}/σ_y, a representative strain ε_R needs to be identified such that the following function is essentially independent of n:

$$\frac{C}{\sigma_R\langle\varepsilon_R\rangle} = \Pi_{\alpha,\frac{\sigma_{res}}{\sigma_y}}\left(\frac{E}{\sigma_R\langle\varepsilon_R\rangle}\right). \tag{8}$$

The functional form of Eq. (8) can be determined through extensive finite element simulations, where ε_R must be determined for each value of residual stress and indenter shape, and so is the fitting function $\Pi_{\alpha,\frac{\sigma_{res}}{\sigma_y}}$.

The approach outlined above, resulting in Eq. (8), involves significantly more effort than using the classical theory summarized in Eq (1)–(2). However, without the help of the representative strain, the material elastic-plastic properties would have to be solved from series of equations like (4), which involves a complicated numerical procedure to solve for multiple unknown material variables from multiple equations. Such approach becomes even more complicated and also prone to error when a residual stress is involved (Chen et al., 2006; Cheng and Cheng, 2004; Wang et al., 2005; Wang and Rokhlin, 2005; Zhao et al., 2006a,b). When using an approach including the representative strain, the apparent number of unknown variables is reduced to only one parameter which can be determined fairly easily and accurately from just one equation (Eq. (8)). The effectiveness of the representative strain approach on stress-free specimens has been well demonstrated (Cao and Lu, 2004; Chollacoop et al., 2003; Dao et al., 2001; Ogasawara et al., 2005, 2006a,b).

1.4. Approach to evaluate material with strain hardening and residual stress

The most common and fundamental residual stress component in coatings is the in-plane equi-biaxial residual stress typically caused by lattice spacing mismatch and thermal expansion mismatch between the coating and substrate. In this paper, we focus on determining the plastic property of the specimen when its modulus and residual stress are known *a priori*. In principle, if the thermal expansion mismatch between the coating and substrate and the elastic modulus of the coating are known, the equi-biaxial residual stress of the coating can be estimated. Therefore, under the premise that there is a known residual stress in the coating, the findings of this paper can be used to correctly assess the plastic properties of the coating by incorporating the effects of residual stress. We also note that as will become evident from the following presentation, the problem can easily be recast into solving for any two unknown of the four indentation parameters (Young's modulus, E, residual stress, σ_{res}, yield strength, σ_y, and work-hardening coefficient n). Although the paper focuses on the effect of equi-biaxial residual stress, the approach is transferable to other forms of residual stresses and will be subjected to study in future work.

The basic premises in this work is that the definition and use of the representative strain outlined in the previous section should still hold when the indented material is subjected to an equi-biaxial residual stress, allowing us to investigate the effect of both strain hardening and residual stress in a straightforward and efficient way. This important assumption, has not been verified before (to our knowledge). The particular value of representative strain that will normalize Eq. (4) into Eq. (8) has itself no direct physical interpretation and thus must be determined for each combination of residual stress. In the following, we will investigate if it is possible to use the concept of representative strain when the test sample is subjected to residual stress, and if the modified Eq. (8) can be used to determine the yield strength and work-hardening coefficient.

2. Numerical simulations

2.1. Finite element model

The functional form of Eq. (8) is achieved through extensive finite element simulations. The simulations were performed using the commercial code ABAQUS (Abaqus, 2004) on intel based workstations. The rigid indenter was simulated using the "rigid contact surface" option. The simulations assumed large deformations

and strains (''non-linear geometry''). The indentation was modeled through an axisymmetric formulation, with a mesh containing more than 5000, 8-node elements. The constitutive behavior follows the power-law described in Eq. (3) with yielding according to the von Mises hypothesis. Coulomb's friction law is used between the contact surfaces, assuming the coefficient of friction to be 0.1. (The friction of coefficient has only a minor influence in indentation (Mesarovic and Fleck, 1999)). To impose an equi-biaxial residual stress, an assumed thermal expansion coefficient is used and the stresses are achieved through imposing proper boundary conditions and changing the temperature accordingly. After the residual stress is imposed in the model, the numerical indentation is conducted.

A broad range of possible materials combinations are investigated by varying Young's modulus, E, residual stress, σ_{res}, yield strength, σ_y, and work-hardening coefficient n. Moreover, three angles of the indenter are investigated, $\alpha = 60°$,63.14°, and 70.3°. The first indenter tip is the commercially available Rockwell tip, and the third one induces the same indentation force-displacement curve as the widely used Berkovich indenter tip (Cheng and Cheng, 2004). The second conical indenter generates force-displacement curves similar to that of a pyramid with triangle 110° which is smaller than that of Berkovich (115°) and also commercially available; the indenter is also used in (Ogasawara et al., 2005). The justification of using three indenter shapes will be apparent in the following. In order to cover a broad range of engineering materials, we investigate a broad spectrum of possible material combinations. To this end we combine $E/\sigma_y = \{10, 20, 50, 100, 200, 500, 1000\}$ with $n = \{0, 0.1, 0.2, 0.3, 0.4, 0.5\}$ and $\sigma_{\text{res}}/\sigma_y = \{\pm 1, \pm 0.8, \pm 0.6, \pm 0.4, \pm 0.2, 0\}$. In all, almost 1400 simulations were needed.

2.2. Numerical results

2.2.1. The effect of residual stress and strain hardening on an indentation test

We have in a previous paper shown that the stress and strain field caused by the indentation strongly interacts with the pre-existing stress field (Chen et al., 2006). This will in turn affect the apparent hardness and stiffness, resulting in that Eq (1)–(2) are not valid when evaluating the tests. The previous study (Chen et al., 2006) only considered a material with perfect plastic ($n = 0$), which will be extended to include $n > 0$ in this study.

Sample force-displacement curves obtained during the (virtual) indentation tests are shown in Fig. 4. For a given material (i.e., given E, σ_y and n) a residual compressive stress results in a higher indentation force for fixed displacement depth, whereas a residual tensile stress results in a lower indentation force, relative a stress free substrate, Fig. 4(a). Similarly, for a given residual stress, the indentation force for a fixed indentation depth increases with increasing work-hardening coefficient, Fig. 4(b) (assuming that E and σ_y are constant). Also, for a given residual stress and work-hardening coefficient, the indentation force for a given indentation depth increases by using a larger half apex angle of the indenter, Fig. 4(c).

In order to verify that the normalized indentation load, C, is indeed independent of the indentation depth, δ, the normalized indentation is plotted as a function of indentation depth in Fig. 5. For the various level of residual stresses investigated, it is evident that C is indeed independent of δ.

Additional insight may be found by investigating the effective (normalized) stresses, $\bar{\sigma}/\sigma_y$, where $\bar{\sigma} = \frac{1}{\sqrt{2}}[(\sigma_1 - \sigma_2)^2 + (\sigma_2 - \sigma_3)^2 + (\sigma_3 - \sigma_1)^2]^{1/2}$ at maximum indentation depth, Fig. 6. In Fig. 6, a range of cases are investigated: the rows correspond to constant residual stress (top row: tensile residual stress, middle row: absent residual stress, and bottom row: compressive residual stress) whereas the columns correspond to constant strain hardening (from left to right: $n = 0$, $n = 0.3$, and $n = 0.5$, respectively). It is seen that the stresses at maximum indentation load increases with increasing strain hardening, as was expected from Fig. 4 where the force increases with increasing strain hardening. This, of course, follows directly from the stress-strain response, where a larger strain hardening coefficient corresponds to a higher stress for a given strain. Thus, the apparent hardness increases with increasing strain hardening since additional force must be applied to reach the same indentation depth. Moreover, the sense of the residual stress has a significant effect on the response, with the residual tensile stresses in general leading to an overall higher state of stress than compressive residual stresses (Fig. 6). These results are in agreement with our previous work (Chen et al., 2006) where a more detailed discussion of the influence of residual stresses may be found.

When evaluating the force-displacement diagrams obtained from indentation testing, it is important to note that some material and residual stress combinations can result in similar response (Alkorta et al., 2005; Tho

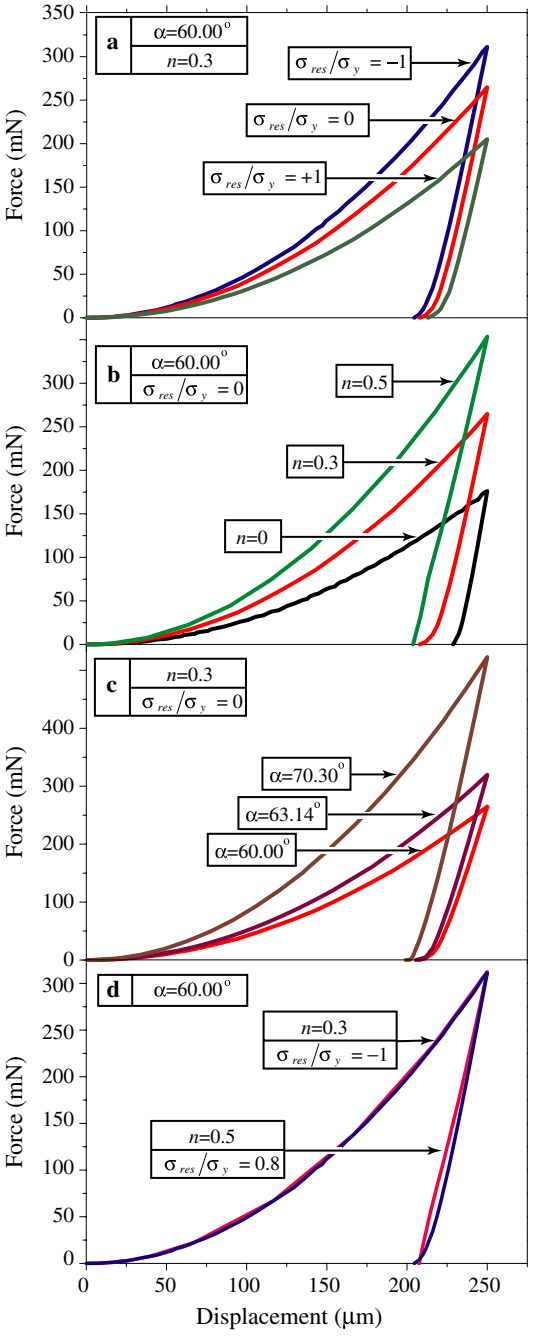

Fig. 4. For the case of $E/\sigma_y = 100$, force-displacement curves from finite element simulations of indentations: (a) for $\alpha = 60°$, σ_{res} / $\sigma_y = \{-1, 0, 1\}$, $n = 0.3$; (b) for $\alpha = 60°$, $\sigma_{res}/\sigma_y = 0$ and $n = \{0,0.3,0.5\}$; (c) for $\alpha = 60°$, 63.14°, and 70.3°, $\sigma_{res}/\sigma_y = 0$ and $n = 0.3$; and (d) for $\alpha = 60°$, two different n and σ_{res}/σ_y show nearly identical force-displacement curves.

et al., 2004). For example, Fig. 4(d) show the case of $\alpha = 60°$, for two cases. Even though the strain hardening coefficient and the residual stresses are not the same, the force-displacement curves are almost identical (in particular within the resolution of a real test). Thus, care must be taken when evaluating the results. One way to avoid erroneous evaluation is to use a set of indenter with various shapes. Thus, we will use three indentation shapes, with $\alpha = 60°$,63.14°, and 70.3°, as was mentioned previously. This will reduce the likelihood of selecting wrong properties based on apparently similar indentation results.

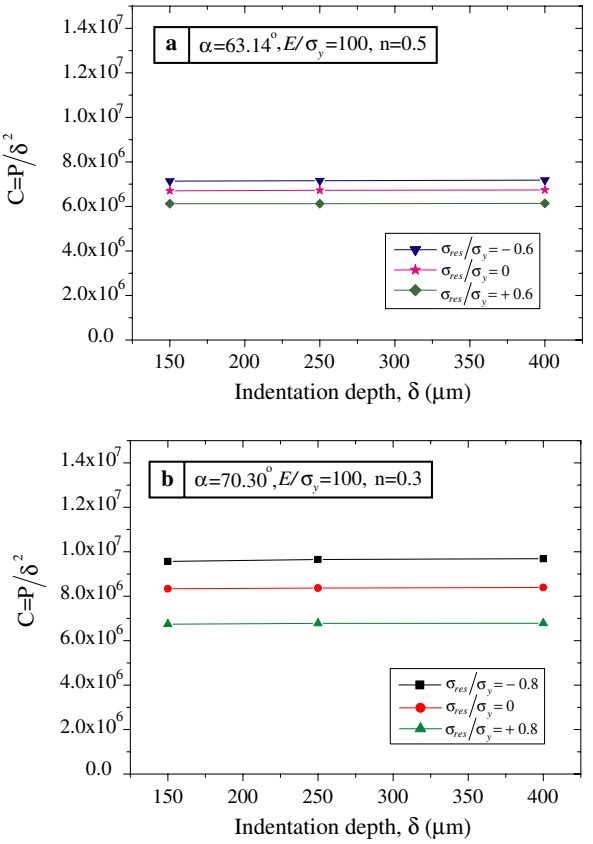

Fig. 5. The normalized indentation load, C, as a function of indentation depth δ for $E/\sigma_y = 100$: (a) $\alpha = 63.14°$ and (b) $\alpha = 70.3°$

2.2.2. Determining the representative strain

As was previously mentioned, (Ogasawara et al., 2005) showed that—absent residual stress—the optimum value of the representative strain for a Berkovich indenter ($\alpha = 70.3°$) is $\varepsilon_R = 0.0115$. This value is a special case, valid for $\sigma_{\text{res}} = 0$. If the representative strain approach is applicable to stressed specimens, we must now determine ε_R (σ_{res}), i.e., determine how the representative strain varies with the residual stress.

The representative strain can only be determined numerically for each σ_{res}, since there is neither a direct physical meaning to ε_R, nor a closed form solution available from where the parameter can be extracted. To this end, the function $C/\sigma_R\langle\varepsilon_R\rangle = \Pi_{\alpha,\frac{\sigma_{\text{res}}}{\sigma_y}}(E/\sigma_R\langle\varepsilon_R\rangle)$ in Eq. (8) is first determined by investigating the response from a virtual indentation for a range of work-hardening coefficients. The value of ε_R, resulting in that all curves for the range of n investigated overlaps to the best degree, is then adopted as the representative strain for the σ_{res} considered. This is obtained by minimizing the difference between the functions, using the principle of "golden section search" and parabolic interpolation.

Sample curves of $C/\sigma_R\langle\varepsilon_R\rangle = \Pi_{\alpha,\frac{\sigma_{\text{res}}}{\sigma_y}}(E/\sigma_R\langle\varepsilon_R\rangle)$ are presented in Figs. 7 and 8. $C/\sigma_R\langle\varepsilon_R\rangle$ for the three indenter shapes investigated (for the case of $\sigma_{\text{res}}/\sigma_y = 0.2$) are shown in Fig. 7(a). Here, the representative strain is $\varepsilon_R = 0.0237$, 0.0223, and 0.0136 for $\alpha = 60°$, 63.14°, and 70.3°, respectively. In Figs. 8(a)–(e), $C/\sigma_R\langle\varepsilon_R\rangle$ is displayed for half apex angle $\alpha = 70.3°$ for a range of $\sigma_{\text{res}}/\sigma_y$. The representative strain for all cases investigated is listed in Table 1 and visualized in Fig. 9. It may be seen that, for compressive residual stresses, the representative strain is almost constant, but increases significantly with the residual stress for tensile residual stress. In (Ogasawara et al., 2005), the representative strain was determined as $\varepsilon_R = 0.0115$ for $\alpha = 70.3°$ Our value deviates somewhat from these values, probably due to the selection of the investigated region of E/σ_y.

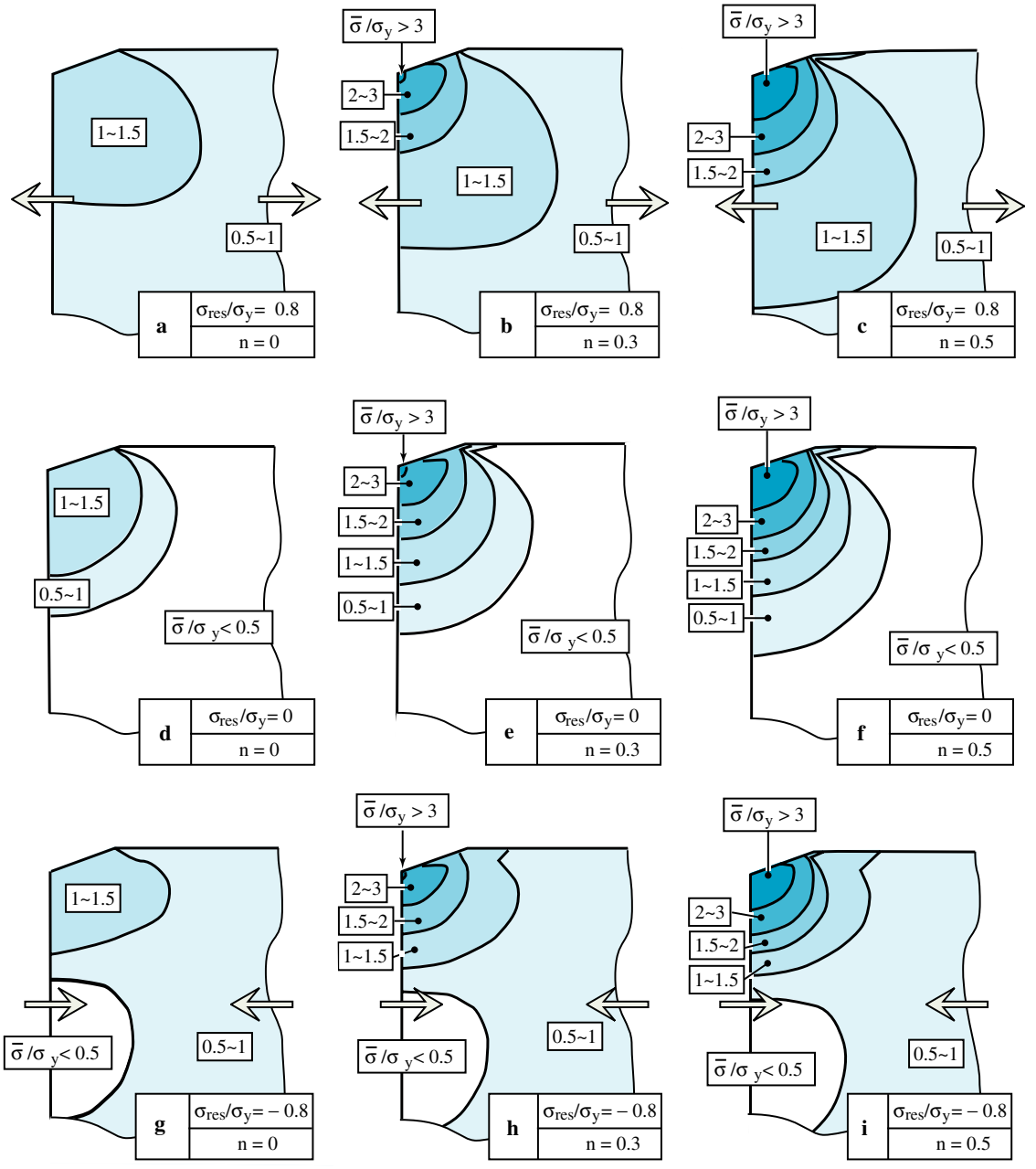

Fig. 6. Equivalent, normalized Mises stresses ($\bar{\sigma}/\sigma_y$) at maximum indentation for $\alpha = 70.30°$ and $E/\sigma_y = 50$: For $\sigma_{res}/\sigma_y = 0.8$ (a) $n = 0$, (b) $n = 0.3$, (c) $n = 0.5$; for $\sigma_{res}/\sigma_y = 0$ (d) $n = 0$, (e) $n = 0.3$, (f) $n = 0.5$; and for $\sigma_{res}/\sigma_y = -0.8$ (g) $n = 0$, (h) $n = 0.3$, (i) $n = 0.5$. The arrows indicate the direction of the residual stress (tensile in the top row, compressive in the bottom row).

2.2.3. Functional form of $\Pi_{\alpha,\frac{\sigma_{res}}{\sigma_y}}$

If the functional form of $\Pi_{\alpha,\frac{\sigma_{res}}{\sigma_y}}$ can be determined, this can serve as the basis for a reverse analysis where experimental results are used as input to determine the material properties. (Ogasawara et al., 2005) showed that it is more convenient to rewrite the function to depend on $\ln E/\sigma_R\langle\varepsilon_R\rangle$), that is

$$\frac{C}{\sigma_R\langle\varepsilon_R\rangle} = \bar{\Pi}_{\alpha,\frac{\sigma_{res}}{\sigma_y}}\left(\ln\frac{E}{(\sigma_R\langle\varepsilon_R\rangle)}\right). \tag{9}$$

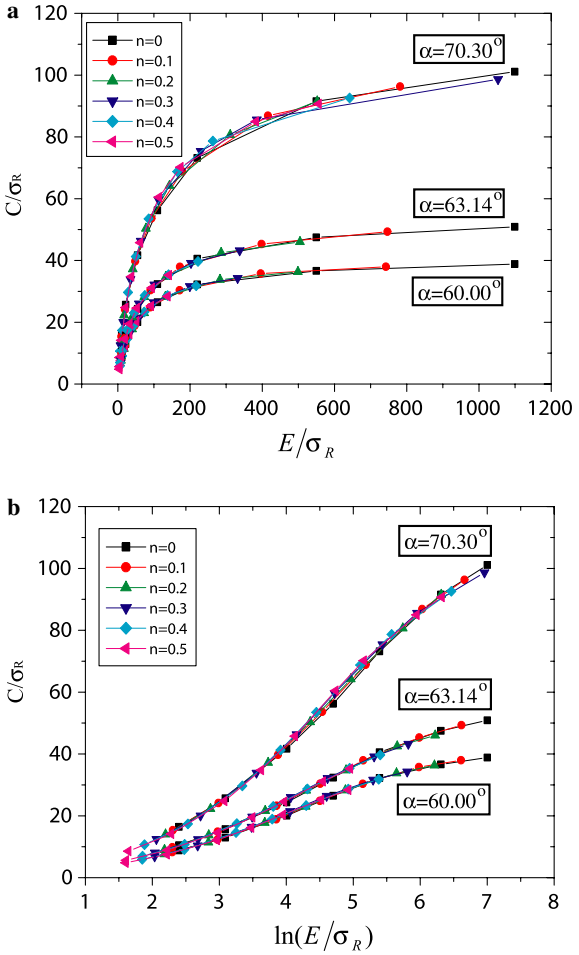

Fig. 7. For the three indenter shapes investigated, normalized indentation load $C/\sigma_R\langle\varepsilon_R\rangle$: (a) as a function of the inverse normalized representative stain $E/\sigma_R\langle\varepsilon_R\rangle$; and (b) as a function of the logarithm of inverse normalized representative strain $\ln E/\sigma_R\ \langle\varepsilon_R\rangle$). ($\sigma_{res}/\sigma_y = 0.2$).

The dimensionless load function takes the form as shown in Figs. 7(b) and 8(f)–(j) and can be fitted into a function of the following form:

$$\frac{C}{\sigma_R\langle\varepsilon_R\rangle} = a_1\left(\ln\frac{E}{\sigma_R\langle\varepsilon_R\rangle}\right)^3 + a_2\left(\ln\frac{E}{\sigma_R\langle\varepsilon_R\rangle}\right)^2 + a_3\left(\ln\frac{E}{\sigma_R\langle\varepsilon_R\rangle}\right) + a_4, \tag{10}$$

where a_i, $i = 1$–4 are constants, determined empirically. Eq. (10) is valid for one specific indenter shape and one specific residual stress. The dependence of residual stress can be functionalized, following a general form of

$$a_i = A_{i1}\left(\frac{\sigma_{res}}{\sigma_y}\right)^3 + A_{i2}\left(\frac{\sigma_{res}}{\sigma_y}\right)^2 + A_{i3}\left(\frac{\sigma_{res}}{\sigma_y}\right) + A_{i4}. \tag{11}$$

Fig. 8. For $\alpha = 70.30°$, normalized indentation load $C/\sigma_R\langle\varepsilon_R\rangle$ as a function of the inverse normalized representative stain $E/\sigma_R\langle\varepsilon_R\rangle$ for (a) $\sigma_{res}/\sigma_y = -0.8$, (b) $\sigma_{res}/\sigma_y = -0.4$, (c) $\sigma_{res}/\sigma_y = 0$, (d) $\sigma_{res}/\sigma_y = 0.4$, (e) $\sigma_{res}/\sigma_y = 0.8$; and $C/\sigma_R\ \langle\varepsilon_R\rangle$ as a function $\ln E/\sigma_R\langle\varepsilon_R\rangle$) [including the fit of Eq. (10)] for (f) $\sigma_{res}\ /\sigma_y = -0.8$, (g) $\sigma_{res}/\sigma_y = -0.4$, (h) $\sigma_{res}\ /\sigma_y = 0$, (i) $\sigma_{res}/\sigma_y = 0.4$, (j) $\sigma_{res}\ /\sigma_y = 0.8$.

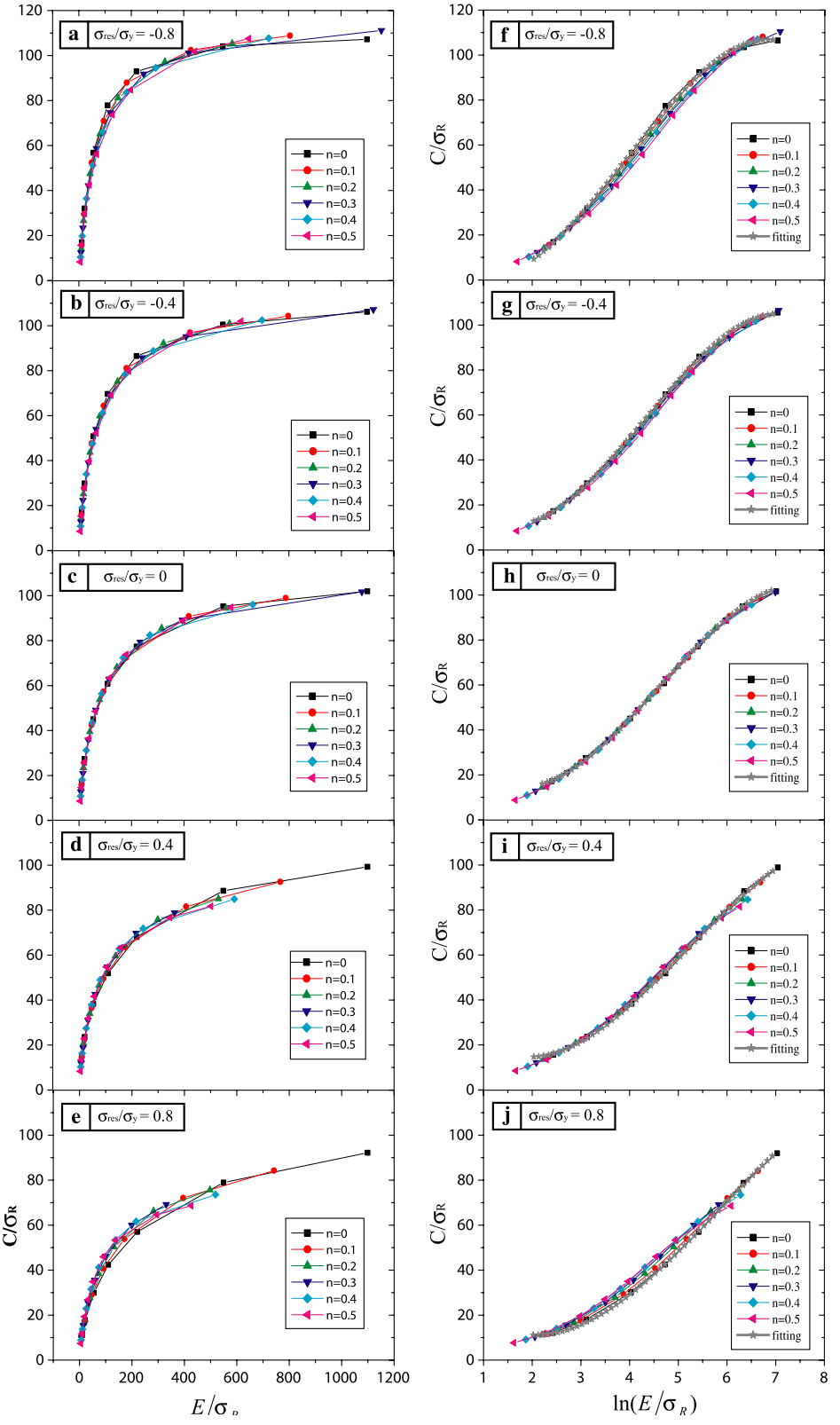
a σres/σy = -0.8
b σres/σy = -0.4
c σres/σy = 0
d σres/σy = 0.4
e σres/σy = 0.8
f σres/σy = -0.8
g σres/σy = -0.4
h σres/σy = 0
i σres/σy = 0.4
j σres/σy = 0.8
n=0
n=0.1
n=0.2
n=0.3
n=0.4
n=0.5
fitting
C/σR
E/σR
ln(E/σR)

Table 1
For the three indenter shapes investigated the representative strain and the parameters of the fitting function for normalized indentation force, Eq. (10)

60°

$$\varepsilon_R = 0.013763 \times \left(\frac{\sigma_{res}}{\sigma_y}\right)^3 + 0.018330 \times \left(\frac{\sigma_{res}}{\sigma_y}\right)^2 + 0.0083056 \times \left(\frac{\sigma_{res}}{\sigma_y}\right) + 0.021068$$
$$a_1 = -0.084897 \times \left(\frac{\sigma_{res}}{\sigma_y}\right)^3 + 0.23559 \times \left(\frac{\sigma_{res}}{\sigma_y}\right)^2 - 0.14846 \times \left(\frac{\sigma_{res}}{\sigma_y}\right) - 0.34485$$
$$a_2 = 0.94807 \times \left(\frac{\sigma_{res}}{\sigma_y}\right)^3 - 3.1944 \times \left(\frac{\sigma_{res}}{\sigma_y}\right)^2 + 3.2998 \times \left(\frac{\sigma_{res}}{\sigma_y}\right) + 4.155$$
$$a_3 = -2.6705 \times \left(\frac{\sigma_{res}}{\sigma_y}\right)^3 + 13.362 \times \left(\frac{\sigma_{res}}{\sigma_y}\right)^2 - 20.348 \times \left(\frac{\sigma_{res}}{\sigma_y}\right) - 7.9104$$
$$a_4 = 0.67573 \times \left(\frac{\sigma_{res}}{\sigma_y}\right)^3 - 18.985 \times \left(\frac{\sigma_{res}}{\sigma_y}\right)^2 + 30.426 \times \left(\frac{\sigma_{res}}{\sigma_y}\right) + 9.0794$$

63.14°

$$\varepsilon_R = 0.011662 \times \left(\frac{\sigma_{res}}{\sigma_y}\right)^3 + 0.017925 \times \left(\frac{\sigma_{res}}{\sigma_y}\right)^2 + 0.0092783 \times \left(\frac{\sigma_{res}}{\sigma_y}\right) + 0.018575$$
$$a_1 = -0.07852 \times \left(\frac{\sigma_{res}}{\sigma_y}\right)^3 + 0.23684 \times \left(\frac{\sigma_{res}}{\sigma_y}\right)^2 - 0.038037 \times \left(\frac{\sigma_{res}}{\sigma_y}\right) - 0.50305$$
$$a_2 = 0.84384 \times \left(\frac{\sigma_{res}}{\sigma_y}\right)^3 - 3.3172 \times \left(\frac{\sigma_{res}}{\sigma_y}\right)^2 + 2.1872 \times \left(\frac{\sigma_{res}}{\sigma_y}\right) + 6.3882$$
$$a_3 = -2.0205 \times \left(\frac{\sigma_{res}}{\sigma_y}\right)^3 + 14.426 \times \left(\frac{\sigma_{res}}{\sigma_y}\right)^2 - 17.994 \times \left(\frac{\sigma_{res}}{\sigma_y}\right) - 15.319$$
$$a_4 = -0.83219 \times \left(\frac{\sigma_{res}}{\sigma_y}\right)^3 - 21.506 \times \left(\frac{\sigma_{res}}{\sigma_y}\right)^2 + 29.727 \times \left(\frac{\sigma_{res}}{\sigma_y}\right) + 18.025$$

70.30°

$$\varepsilon_R = 0.0055531 \times \left(\frac{\sigma_{res}}{\sigma_y}\right)^3 + 0.0081265 \times \left(\frac{\sigma_{res}}{\sigma_y}\right)^2 + 0.0055779 \times \left(\frac{\sigma_{res}}{\sigma_y}\right) + 0.012195$$
$$a_1 = -0.37865 \times \left(\frac{\sigma_{res}}{\sigma_y}\right)^3 + 0.28257 \times \left(\frac{\sigma_{res}}{\sigma_y}\right)^2 + 0.61774 \times \left(\frac{\sigma_{res}}{\sigma_y}\right) - 0.98458$$
$$a_2 = 4.9742 \times \left(\frac{\sigma_{res}}{\sigma_y}\right)^3 - 4.2095 \times \left(\frac{\sigma_{res}}{\sigma_y}\right)^2 - 5.6722 \times \left(\frac{\sigma_{res}}{\sigma_y}\right) + 13.633$$
$$a_3 = -19.22 \times \left(\frac{\sigma_{res}}{\sigma_y}\right)^3 + 19.469 \times \left(\frac{\sigma_{res}}{\sigma_y}\right)^2 + 7.6312 \times \left(\frac{\sigma_{res}}{\sigma_y}\right) - 39.087$$
$$a_4 = 19.349 \times \left(\frac{\sigma_{res}}{\sigma_y}\right)^3 - 31.654 \times \left(\frac{\sigma_{res}}{\sigma_y}\right)^2 + 4.7804 \times \left(\frac{\sigma_{res}}{\sigma_y}\right) + 46.405$$

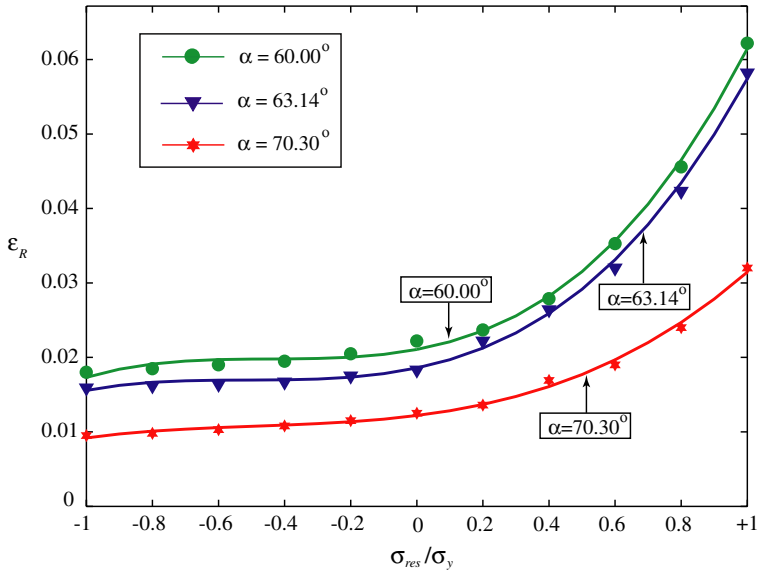

Fig. 9. Representative strain as a function of normalized residual stress for the indenter shapes investigated, showing the cubical fit.

with A_{ij}, $j = 1$–4 being constants determined empirically for each indenter shape. The three sets of Eq. (11)—one for each indenter shape—are presented in Table 1. How the fitted function (10), using the parameters in Table 1, reproduces Eq. (9) is displayed in the right hand column of Fig. 8. An excellent fit is seen.

3. Reverse analysis

To explore how the presence of residual stress affects the indentation measurement, we assume that the residual stress, σ_{res}, and Young's modulus, E, are known for the specimen under investigations, the yield strength, σ_y, and the work-hardening coefficient, n, can now be determined based on indentation tests and inverse analysis, with the effect of residual stress being incorporated. Since we only have one equation [Eq. (10)] but two unknowns (σ_y and n), two indentations experiments with different shaped indenter tip are needed

to solve for the two unknown material parameters. From the numerical simulations, we have seen that using results from three different shaped indenters give significantly more accurate material properties. As noted previously, the problem can easily be recast into solving for any two combinations of the indentation parameter, i.e., any two of σ_{res}, E, σ_y, n.

The principle of the reverse analysis is summarized by a schematic flow chart in Fig. 10, and can be described with the following synopsis: Based on an indentation test, $C \equiv P/\delta_{max}^2$ is determined and serves—together with the known residual stress, σ_{res}, and Young's modulus, E—as input to the reverse analysis. Additional input to the analysis is an estimated value of the yield strength, σ_{y0}. From Table 1, the corresponding representative strain ε_R and the constants a_i, $i = 1$–4 of Eq. (10) are interpolated (by linear interpolation), whereupon the representative stress $\sigma_R\langle\ \varepsilon_R\rangle$ can be determined for each of the three investigated indenter shapes. Based on the obtained representative stress and strain, the corresponding material parameters σ_y and n can be deduced uniquely and are selected as the average of the three possible combinations of the investigated indenter-shapes. As mentioned above, only two shapes are needed to determine the two unknowns. However, if all three shapes are used, three combinations of two are possible. By selecting the average value, these three combinations result in both a faster convergence and in more accurate material parameters. Final-

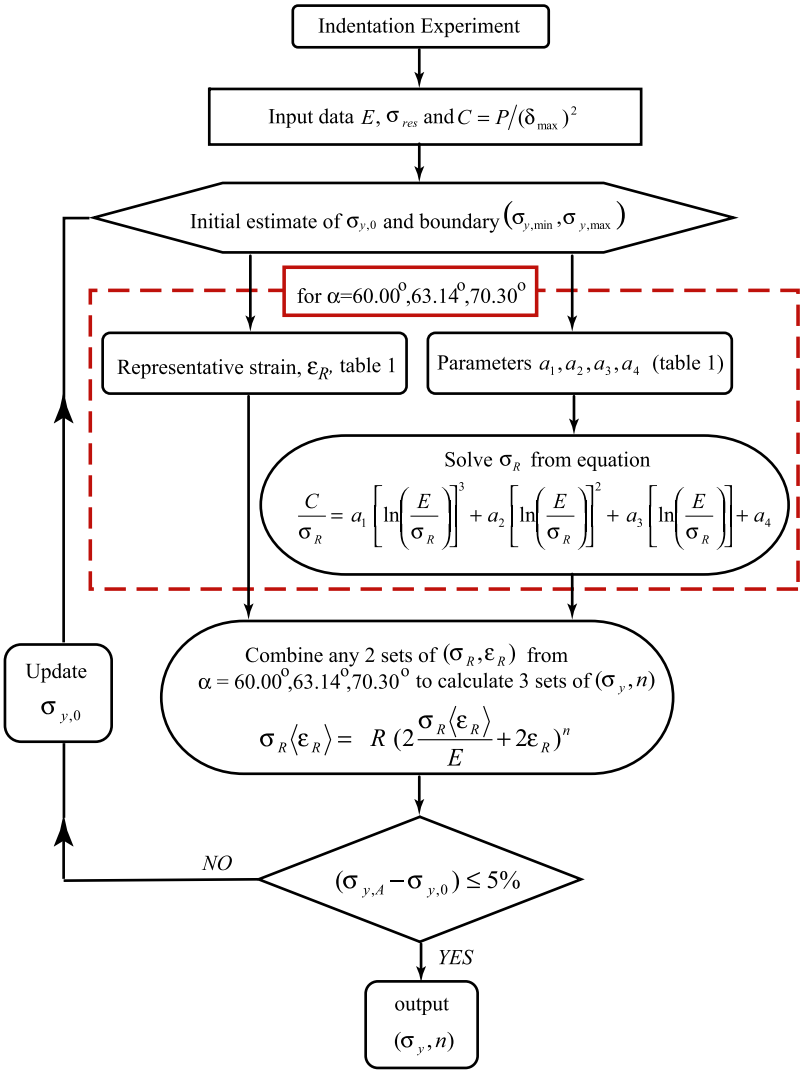

Fig. 10. Schematic of the reverse analysis.

ly, the yield strength obtained in the last step, σ_{yA}, is compared to the initially assumed yield strength σ_{y0}. If $|\sigma_{yA} - \sigma_{y0}| <$ error (we used max 5% error), then a solution is found, where $\sigma_y = \sigma_{yA}$ and n are the material properties of the test specimen. If $|\sigma_{yA}$-$\sigma_{y0}| >$ error, then a new σ_{y0} is selected and the routine is reiterated. In our implementation, we used the predefined function *fminbnd* in MATLAB (Matlab, 2004) to update σ_{y0}. This routine minimizes a function [in our case $|\sigma_{yA\ -\ \sigma_{y0}}| <$ error, based on a set of conditions (here the center part of the flow chart) for a given interval [here $(\sigma_{y\,\min}, \sigma_{y\,\max})$].

The numerical accuracy of the reverse analysis is investigated by conducting a set of numerical indentations of material properties *not* used to determine the coefficients a_i, $i = 1$–4 to Eq. (10) (as listed in Table 1). For the given set of input parameters, a numerical indentation testing is conducted, and $C \equiv P/\delta^2_{\max}$ is determined. This is then used in the reverse analysis to determine σ_y and n. The results for the selected set of material parameters are shown in Fig. 11 and it can be seen that a good reproduction of the data is achieved, with errors less than 5%.

In addition, we compare to "real" material data based on material data available Kim et al., 2006. In that paper, indentations matching our proposed method are unfortunately not presented, but we select to utilize their material database, since it contains the needed set of parameter with the purpose of investigating the more realistic material properties than Fig. 11 presented. These "real" material data are summarized in Table 2. In this case, we again conduct virtual experiments, assuming selected magnitudes of residual stress. Based on $C \equiv P/\delta^2_{\max}$ obtained from the numerical simulation, we determine σ_y and n, presented in Table 2. Here, all errors are less than 5%. For Tool steel SKH51 (Kim et al., 2006) the stress-strain response according the constitutive Eq. (3) is plotted in Fig. 12. The original data is compared to the data obtained thought the reverse

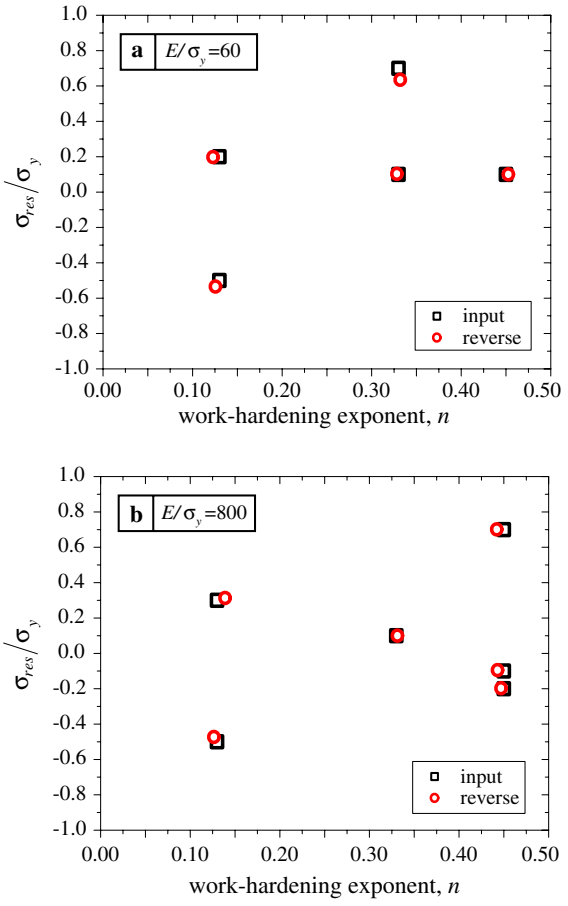

Fig. 11. Comparison between predicted results based on the reveres analysis and the input parameters in the numerical simulation.

Table 2
Sample results of the reverse analysis from virtual experiments for a range of materials

Material	Input						Reverse analysis results	
	E (GPa)	σ_y (MPa)	n	v	E/σ_y	σ_{res}/σ_y	σ_y (MPa)	n
SKH51 Toll steel	246.80	263.85	0.2591	0.2411	935.38	−0.2	267.60	0.2567
						0.3	260.45	0.2579
						−0.5	272.37	0.2572
S45C structural steel	209.05	374.14	0.3378	0.2873	558	0.2	380.99	0.3348
						−0.4	380.32	0.3404
NAK plastic mold steel	202.62	1207.44	0.0508	0.2868	167	0.4	1210.14	0.0642

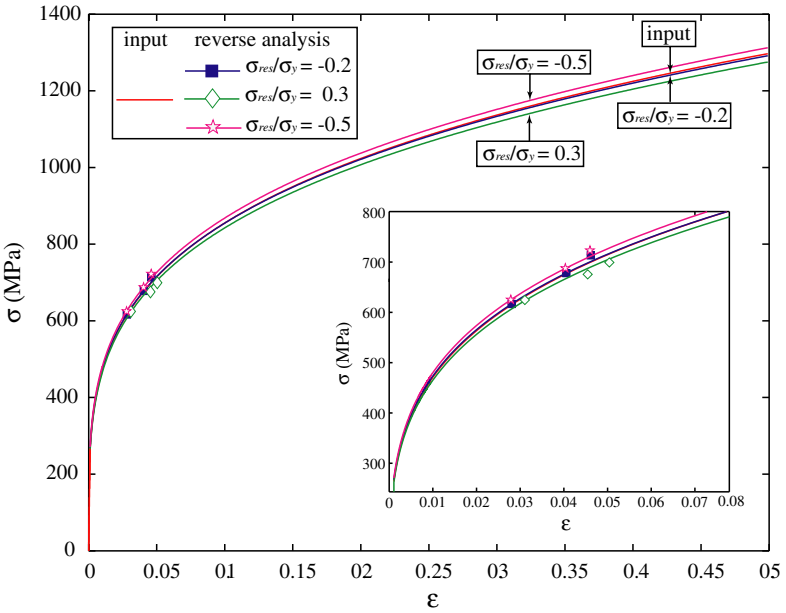

Fig. 12. Comparison of the true and the predicted stress-strain curve, based on the reverse analysis and the input parameters, for Tool steel SKH51. The insert shows an enlargement of the stress-strain curve for stresses between 300 and 800 MPa. The markers indicate the pair of representative stress and strain for the three indenter shapes used. The results for $\sigma_{res}/\sigma_Y = -0.2$ overlaps the input curve within the resolution of the figure.

analysis. In this plot, the markers indicate the pair of the representative stress and strain for the three indenter shapes used. An excellent agreement between the curves predicted from the virtual experiments using our proposed method and the true curves are obtained, Fig. 12. Thus, in our new approach, including both the effect of residual stress and strain hardening, the calculated plastic behavior is predicted reasonable well, regardless of the stress state in the material.

The next step is to compare this method to experimental investigations. Work is currently ongoing in our laboratory to verify the model developed herein, but is not completed yet. Unfortunately, comparing to published data is not possible, since we have not found a complete set of experiments needed to conduct the revere analysis.

4. Concluding remarks

A technique for evaluating instrumented indentation testing of materials that exhibits strain hardening after yielding and which are subjected to a pre-existing equi-biaxial stress field is presented. The technique is based on conducting two or—for better accuracy—three indentation tests, and through a reverse analysis uniquely

determine two unknown plastic parameters. The indentation tests are assumed to be conducted with three conical indenters with the half apex angle of $\alpha = 60°$,63.14°, and 70.3°, which are all commercially available.

The core of the proposed technique is based on identifying the "representative strain," ε_R, where we have adopted the definition of representative strain presented by Ogasawara et al. (2005). The representative strain maps the response from indentation testing of the various materials (e.g., different Young's modulus, yield strength and strain hardening) into depending only on one parameter: the normalized Young's modulus. In this case, Young's modulus is normalized with respect to the "representative stress," which can be directly related to the representative strain. Previously, several authors have shown that expressing the results from indentation testing in terms of representative strain and representative stress is an effective method to evaluate indentation testing of materials that exhibits significant strain hardening during yielding. In this paper, we show that this technique can be extended and used when the material is subjected to an equi-biaxial residual stress. However, each level of residual stress is associated with one representative strain.

The representative strain only can be determined empirically, based on numerical simulations of indentation tests. Thus, a significant effort in this work has been to determine the representative strain for the each level of residual stress within the range investigated. The numerical simulations were conducted with finite element simulations, simulating indentation testing on a range of materials and levels of residual stress in order to determine the representative strain. Based on these simulations, a dimensionless function describing the indentation force and the displacement is identified and expressed in an empirical form. This function, $\bar{\Pi}_{\alpha,\frac{\sigma_{res}}{\sigma_y}}$, along with the representative stress are the two functions used in the reverse analysis to determine the unknown properties. Similar dimensionless functions are constructed for each of the three indenter angles.

We have shown that the concept of representative strain can be used when a residual stress is present. To this end, we presented a solution where Young's modulus and the residual stress are assumed known (which is typical for coatings), and the yield strength and strain hardening are determined uniquely based on the indentation testing and reverse analysis. However, with the set of equations presented herein, any two combinations of the four parameters Young's modules, residual stress, yield strength and strain hardening can be determined, by slightly modifying the proposed evaluation scheme.

Acknowledgements

J.Y. and A.M.K. acknowledge that this work was supported by ONR-N00014-04-1-0498 and NSF DMR-0346664. X.C. was supported by NSF CMS-0407743.

References

Abaqus, 2004. Abaqus 6.5, Pawtucket, Rhode Island, ABAQUS Inc.

Alkorta, J., Martinez-Esnaola, J., Sevillano, J., 2005. Absence of one-to-one correspondence between elastoplastic properties and sharp-indentation load-penetration data (vol 20, pg. 432, 2005). Journal of Materials Research 20 (5), 1369.

Atkins, A., Tabor, D., 1965. Plastic indentation in metals with cones. Journal of the Mechanics and Physics of Solids 13 (3), 149–164.

Cao, Y., Lu, H., 2004. A new method to extract the plastic properties of metal materials from an instrumented spherical indentation loading curve. Acta Materialia 52 (13), 4023–4032.

Carlsson, S., Larsson, P.L., 2001a. On the determination of residual stress and strain fields by sharp indentation testing. Part I: theoretical and numerical analysis. Acta Materialia 49 (12), 2179–2191.

Carlsson, S., Larsson, P.L., 2001b. On the determination of residual stress and strain fields by sharp indentation testing. Part Ii: experimental investigation. Acta Materialia 49 (12), 2193–2203.

Chen, M.W., Ott, R., Hufnagel, T.C., Wright, P.K., Hemker, K.J., 2003. Microstructural evolution of platinum modified nickel aluminide bond coat during thermal cycling. Surface and Coatings Technology 163, 25–30.

Chen, X., Yan, J., Karlsson, A.M., 2006. On the determination of residual stress and mechanical properties by indentation. Materials Science and Engineering: A 416 (1–2), 139–149.

Cheng, Y., Cheng, C., 2004. Scaling, dimensional analysis, and indentation measurements. Materials Science and Engineering R 44 (4-5), 91–149.

Cheng, Y.T., Cheng, C.M., 1998. Scaling approach to conical indentation in elastic-plastic solids with work hardening. Journal of Applied Physics 84, 1284–1291.

Chollacoop, N., Dao, M., Suresh, S., 2003. Depth-sensing instrumented indentation with dual sharp indenters. Acta Materialia 51 (13), 3713–3729.

Dao, M., Chollacoop, N., Vanvliet, K.J., Venkatesh, T.A., Suresh, S., 2001. Computational modeling of the forward and reverse problems in instrumented sharp indentation. Acta Materialia 49, 3899–3918.

Eriksson, C., Larsson, P., Rowcliffe, D., 2003. Strain-hardening and residual stress effects in plastic zones around indentations. Materials Science and Engineering A-Structural Materials Properties Microstructure and Processing 340 (1–2), 193–203.

Fleck, N.A., Hutchinson, J.W., 1997. Strain gradient plasticity. Advances in Applied Mechanics 33, 295–361.

Hay, J.C., Bolshakov, A., Pharr, G.M., 1999. A critical examination of the fundamental relations used in the analysis of nanoindentation data. Journal of Materials Research 14 (6), 2296–2305.

Johnson, K.L., 1985. Contact Mechanics. Cambridge University Press, Cambridge.

Karlsson, A.M., Evans, A.G., 2001. A numerical model for the cyclic instability of thermally grown oxides in thermal barrier systems. Acta Materialia 49 (10), 1793–1804.

Karlsson, A.M., Levi, C.G., Evans, A.G., 2002. a model study of displacement instabilities during cyclic oxidation. Acta Materialia 50 (6), 1263–1273.

Kim, S., Lee, B., Choi, Y., Kwon, D., 2006. Quantitative determination of contact depth during spherical indentation of metallic materials—a fem study. Materials Science and Engineering A-Structural Materials Properties Microstructure and Processing 415 (1–2), 59–65.

Lee, Y.H., Kwon, D., 2003. Measurement of residual-stress by nanoindentation on elastically strained (100) W. Scripta Materialia 49 (5), 459–465.

Lee, Y.H., Kwon, D., 2004. Estimation of biaxial surface stress by instrumented indentation with sharp indenters. Acta Materialia 53 (6), 1555–1563.

Lichinchi, M., Lenardi, C., Haupt, J., Vitali, R., 1998. Simulation of berkovich nanoindentation experiments on thin films using finite element method. Thin Solid Films 312, 240–248.

Matlab, 2004. Matlab 7.0, The MathWorks Incorporate.

Mesarovic, S.D., Fleck, N.A., 1999. Spherical indentation of elastic-plastic solids. Proceedings of the Royal Society London A455, 2707–2728.

Ogasawara, N., Chiba, N., Chen, X., 2005. Representative strain of indentation analysis. Journal of Materials Research 20 (8), 2225–2234.

Ogasawara, N., Chiba, N., Chen, X., 2006a. Limit analysis-based approach to determine the material plastic properties with conical indentation. Journal of Materials Research 21 (4), 947–957.

Ogasawara, N., Chiba, N., Chen, X., 2006b. Measuring the plastic properties of bulk materials by single indentation test. Scripta Materialia 54 (1), 65–70.

Oliver, W.C., Pharr, G.M., 1992. An improved technique for determining hardness and elastic- modulus using load and displacement sensing indentation experiments. Journal of Materials Research 7 (6), 1564–1583.

Pan, D., Chen, M.W., Wright, P.K., Hemker, K.J., 2003. Evolution of a diffusion aluminide bond coat for thermal barrier coatings during thermal cycling. Acta Materialia 51 (8), 2205–2217.

Suresh, S., Giannakopoulos, 1998. A new method for estimating residual stresses by instrumented sharp indenter. Acta Materialia 46 (16), 5755–5767.

Swadener, J.G., Taljat, B., Pharr, G.M., 2001. Measurement of residual stress by load and depth sensing indentation with spherical indenters. Journal of Materials Research 16, 2091–2102.

Tabor, D., 1951. Hardness of Metals. Oxford University Press, New York.

Tho, K., Swaddiwudhipong, S., Liu, Z., Zeng, K., Hua, J., 2004. Uniqueness of reverse analysis from conical indentation tests. Journal of Materials Research 19 (8), 2498–2502.

Wang, L., Ganor, M., Rokhlin, S., 2005. Inverse scaling functions in nanoindentation with sharp indenters: determination of material properties. Journal of Materials Research 20 (4), 987–1001.

Wang, L., Rokhlin, S., 2005. Universal scaling functions for continuous stiffness nanoindentation with sharp indenters. International Journal of Solids and Structures 42 (13), 3807–3832.

Xu, Z.-H., Li, Xiaodong, 2005. Influence of equi-biaxial residual stress on unloading behaviour of nanoindentation. Acta Materialia 53, 1913–1919.

Yan, J., Karlsson, A.M., Chen, X., 2007. A new approach to measure equi-biaxial residual stress and elastic-plastic properties by conical micro-indentation. Journal of Engineering Materials and Technology, in press.

Zhao, M., Chen, X., Yan, J., Karlsson, A.M., 2006a. Determination of uniaxial residual stress and mechanical properties by instrumented indentation. Acta Materialia 54, 2823–2832.

Zhao, M., Ogasawara, N., Chiba, N., Chen, X., 2006b. A new approach to measure the elastic-plastic properties of bulk materials using spherical indentation. Acta Materialia 54 (1), 23–32.